Shear- and magnetic-field-induced ordering in magnetic nanoparticle dispersion from small-angle neutron scattering

V. V. Krishnamurthy, A. S. Bhandar, M. Piao, I. Zoto, A. M. Lane, D. E. Nikles, J. M. Wiest, and G. J. Mankey
Center for Materials for Information Technology, The University of Alabama, Tuscaloosa, Alabama 35487

L. Porcar and C. J. Glinka
NIST Center for Neutron Research, National Institute of Standards and Technology, Gaithersburg, Maryland 20899-8562
(Received 17 December 2002; published 23 May 2003)

Small-angle neutron scattering experiments have been performed to investigate orientational ordering of a dispersion of rod-shaped ferromagnetic nanoparticles under the influence of shear flow and static magnetic field. In this experiment, the flow and flow gradient directions are perpendicular to the direction of the applied magnetic field. The scattering intensity is isotropic in zero-shear-rate or zero-applied-field conditions, indicating that the particles are randomly oriented. Anisotropic scattering is observed both in a shear flow and in a static magnetic field, showing that both flow and field induce orientational order in the dispersion. The anisotropy increases with the increase of field and with the increase of shear rate. Three states of order have been observed with the application of both shear flow and magnetic field. At low shear rates, the particles are aligned in the field direction. When increasing shear rate is applied, the particles revert to random orientations at a characteristic shear rate that depends on the strength of the applied magnetic field. Above the characteristic shear rate, the particles align along the flow direction. The experimental results agree qualitatively with the predictions of a mean field model.

DOI: 10.1103/PhysRevE.67.051406 PACS number(s): 82.70.−y, 75.50.Mm, 83.50.Ax, 28.20.Cz

I. INTRODUCTION

Heterogeneous liquids such as dispersions or emulsions can exhibit properties unlike those of any of the constituent phases. They also present the possibility of self-assembly or assisted assembly into materials with ordered structures at the microscale or at the nanoscale. This is particularly true for dispersions containing magnetic particles. Magnetic particle dispersions behave like fluids, but they also respond to magnetic fields [1–3]. For example, the mechanical properties (e.g., viscosity) of a magnetic particle dispersion change drastically under the application of a magnetic field [4]. The unique nature of these liquids as magnetic fluids endows them with a variety of technological applications [5].

For the manufacturing of flexible data storage media [6,7], submicron sized, acicular (rod-shaped) ferromagnetic particles are dispersed in a solvent with a low molecular weight polymer to prevent the particles from flocculating. These dispersions are ferrofluids in the sense that the particles have permanent magnetic moments; however, the particles are about an order of magnitude larger in size than ferrofluid particles and have an acicular shape as opposed to conventional ferrofluid particles that are nearly spherical. The acicular shape of the particles gives them higher magnetic anisotropy for better thermal stability and enables the possibility of controlling particle orientation. A variety of experimental and theoretical studies have been performed on ferrofluids [1], but fewer theoretical and simulation studies have been conducted on dispersions of acicular magnetic particles [8–14]. In the manufacturing of flexible media, both flow and field are applied during the coating process, so it is desirable to understand the influence of these forces on the orientational order of the particles in dispersion.

Here, small-angle neutron scattering (SANS) investigations are reported for a magnetic dispersion of acicular ferromagnetic particles under the influence of steady shear flow and static magnetic field. The experimental results show that initially randomly oriented magnetic particles are oriented in the flow direction in a shear flow. An applied magnetic field orients the particles along the field direction. When shear flow is applied in a direction perpendicular to the direction of the static magnetic field, particles retain their alignment along the magnetic field below a characteristic shear rate $\dot{\gamma}_c$. At $\dot{\gamma}_c$, the particles reattain a random state of order, and they are oriented in the flow direction above this shear rate.

II. EXPERIMENT

The prepared dispersions contained cyclohexanone as a solvent, a commercial antiflocculating polymer (Nippon Zeon Co., MR110) [15], and metal particles. The particles are primarily iron with saturation magnetization of $(750–900)\times10^6$ emu/m^3, coercivity 130–220 mT, specific surface area 42 000 m^2/Kg, average length $L=200$ nm, and average aspect ratio $L/d=8$, where d is the average diameter of the particle. The average density of the particle is 5700 kg/m^3. The particles have a log-normal length distribution with a width of 20%. The MR110 polymer is a polyvinyl chloride–acetate copolymer commonly used for magnetic dispersions. It has 0.7 wt % sulfonic acid groups, 0.6 wt % hydroxyl groups, and 3.0 wt % of an epoxy component. Its weight average molecular weight is 26 000, and its number average molecular weight is 12 000. Adsorption of this polymer onto the particle surfaces provides steric stabilization against agglomeration. Cyclohexanone was chosen as the solvent because of its good solubility for MR110 and for its low volatility.

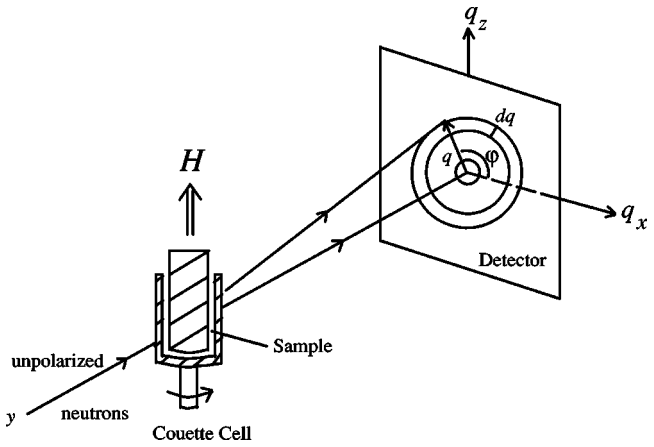

FIG. 1. Schematic view of the experimental setup for SANS with the Couette shear cell and the scattering geometry in the *x*-*z* plane.

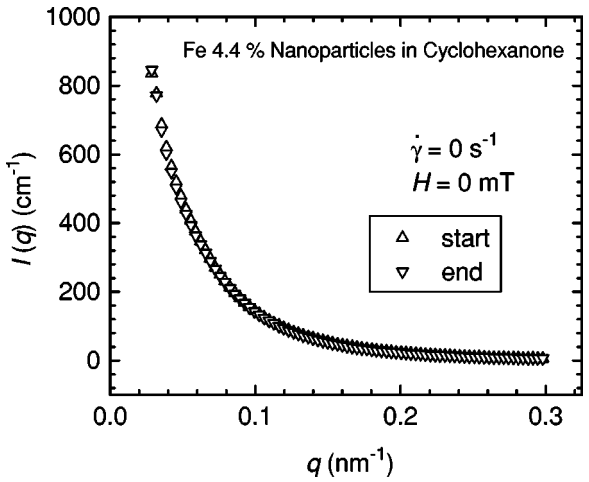

FIG. 2. Scattering intensity I as a function of scattering vector q at zero shear rate and zero applied magnetic field.

The particles, MR110, and part of the cyclohexanone were mixed in a double planetary mixer to make a dough. Then the dough was further dispersed with more cyclohexanone in a sawtooth premixer. Finally, the dispersion was milled in an Eiger mill. The final dispersion contained 4.4% particles by volume (21% by weight) and 3.34% MR110 by weight.

Small-angle neutron scattering experiments were performed using the 30-m SANS instrument NG7 at the NIST Center for Neutron Research, Gaithersburg, Maryland. The dispersion was loaded in a Couette shearing cell [16,17] and the SANS measurements were performed using a wavelength of 6 Å and a sample-to-detector distance of 15.5 m for covering the horizontal q range of 0.029–0.215 nm^{-1}. Figure 1 displays a schematic view of the experimental setup [17]. The shear flow is along the x direction, and the shear rate $\dot{\gamma}$ is given as $\partial v_x/\partial y$, where v_x is the flow velocity. The neutrons were incident on the sample along the y direction in a radial geometry, which is more suitable for detecting particle alignment than the tangential geometry. The magnetic field is applied along the z direction (i.e., perpendicular to the shear flow). The scattered neutrons were detected by an area-sensitive detector in the x-z plane.

Small-angle neutron scattering experiments were first performed in zero-applied magnetic field, while the dispersion was subjected to shear flow. Steady shear flow results were obtained at shear rates ranging from 0 s^{-1} to 4000 s^{-1} by conducting shear rate sweeps wherein the shear rate was increased or decreased in stair-step fashion. Most measurements were conducted in increasing-shear-rate sweeps with the data collection time for each scan being 15 min. Selected decreasing-shear-rate sweeps were also examined in order to investigate the hysteresis in alignment and preshearing effects. In addition, scattering experiments were performed (both with and without shear flow) with a static magnetic field in the z (i.e., neutral or vorticity) direction.

In each case, i.e., at each shear rate, scattering yielded an isointensity plot—a two-dimensional plot of scattering intensity in the x-z plane. As in conventional SANS data reduction, each dataset is corrected for detector background, sensitivity, scattering from the empty cell, and is scaled to absolute units of cross section per unit volume using a direct beam intensity measurement. The scattering asymmetry as a function of the azimuthal angle ϕ, defined in Fig. 1, was obtained by integrating the scattering intensity with an annular average at the scattering vector q of 0.18 nm^{-1} with a width of 0.009 nm^{-1} using the NIST SANS data analysis program [18]. The results are qualitatively the same for all q values. This particular q value was chosen for good azimuthal resolution with a good signal-to-noise ratio.

III. RESULTS

The neutron scattering intensity $I(q)$ as a function of the scattering vector q at zero shear rate at the start of the scan (zero preshear) and at the end of the scan (after shearing to 4000 s^{-1}) is given in Fig. 2. These two curves superimpose quite well in the entire q range. Figure 3 displays the scattering intensity as a function of azimuthal angle, $I(\phi)$, at (a) zero shear rate, zero field, (b) high shear rate of 4000 s^{-1}, zero field, and (c) zero shear rate, high applied field 18 mT. At zero shear rate and zero field [Fig. 3(a)] the intensity is independent of the azimuthal angle ϕ, indicating fully isotropic scattering of neutrons from the dispersion, and suggesting random particle orientation. Under shear flow with no applied field [Fig. 3(b)], the scattering pattern develops an angular dependence. Similarly, the scattering pattern also develops an angular dependence in an applied magnetic field of 18 mT in the absence of shear flow [Fig. 3(c)]. The maxima in Figs. 3(b) and 3(c) are 90° out of phase, indicating a rotation in the average orientation of the particles.

The scattering of neutrons from a magnetic dispersion can have two contributions; a magnetic contribution due to interactions between neutron spin and the local fields of spins and a nuclear contribution due to the interaction between the impinging neutron and nuclei in the dispersion [19]. The magnetic scattering is inherently anisotropic and is strongest in the direction perpendicular to a particle's magnetization axis. The nuclear scattering is present in all directions, but extends to wider scattering angles in the direction perpendicular to

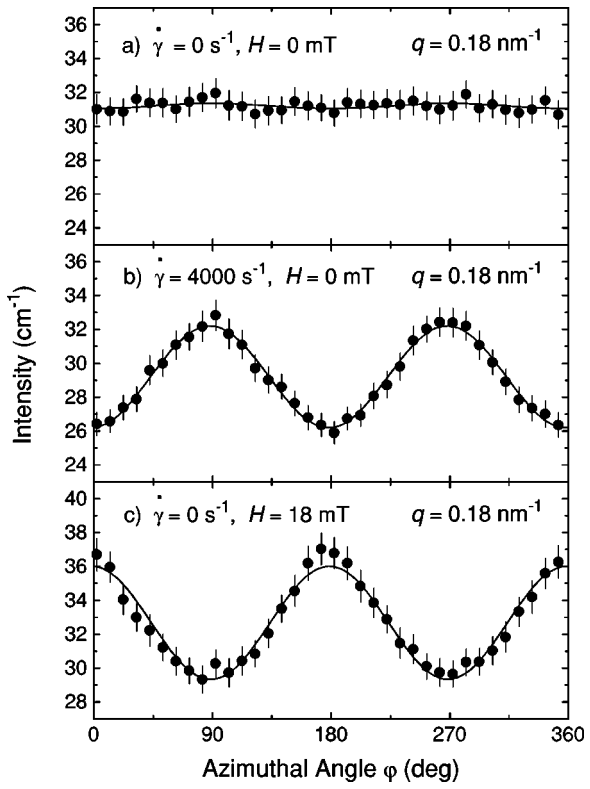

FIG. 3. Intensity as a function of the azimuthal angle ϕ in a 4.4 vol % magnetic dispersion for (a) zero-shear rate, zero field, (b) shear rate of 4000 s^{-1}, zero field, and (c) zero-shear rate, applied field $H=18$ mT.

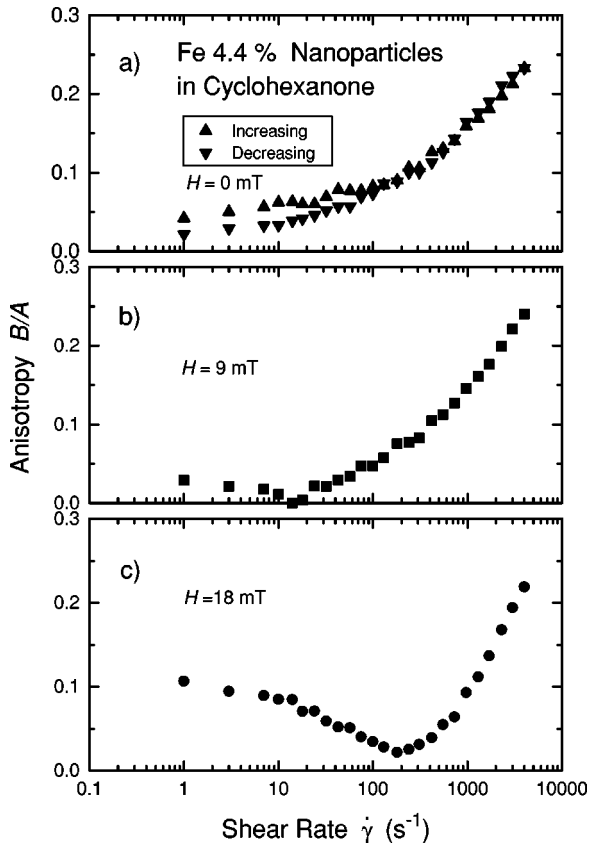

FIG. 4. Anisotropy B/A as a function of shear rate in a 4.4 vol % magnetic dispersion for (a) increasing shear rate sweep with no applied field and decreasing shear rate sweep with no applied field, (b) applied field of 9 mT, and (c) applied field of 18 mT. The error bars are of the order of the size of the symbols.

the long axis of an acicular particle. In the present case, we expect the magnetization axis to coincide with the long axis of the particles. Hence both anisotropic contributions give rise to scattering that is enhanced in the same direction. The resulting anisotropy can, therefore, be associated directly with the average orientation of the particles.

The angular dependence of the scattering intensity can be fitted to

$$I(\phi)=A+B\sin^2(\phi+\psi), \tag{1}$$

where A is the magnitude of the isotropic scattering, B is the amplitude of the anisotropic scattering, and ψ is a phase factor (i.e., the angle between the average direction of the particle alignment and the direction of shear flow). Here we refer to ψ as the tilt angle. The solid lines in Fig. 3 are the best fits of Eq. (1) to the data. We found that A is nearly independent of the shear rate. The ratio B/A gives a measure of the anisotropy of the scattering [20], which indicates the degree of orientation of the particles by externally applied torques, in this case the shear flow and/or the applied magnetic field. For the three cases shown in Fig. 3, we find (a) $B/A=0.01$, $\psi=0°$ (fixed) (b) $B/A=0.23$, $\psi=1.9(2)°$, and (c) $B/A=0.23$, $\psi=91.1(12)°$. The tilt angle of 0° is found to fit the data for the case (a), indicating that the particles are randomly oriented. The value of the tilt angle for the case (b) is too small, so one can say that the particles are well aligned along the direction of shear flow.

Figure 4 displays the anisotropy B/A as a function of shear rate for three values of the applied magnetic field. The anisotropy varies strongly with the shear rate both in zero applied field as well as in an applied field H of 9 and 18 mT. In the absence of magnetic field, the anisotropy increases monotonically with the increase of shear rate, and reaches a value of 0.23 at a shear rate of 4000 s^{-1}. Note that a small anisotropy of 0.01 is observed at zero shear rate in zero-applied field; this is probably within the error limits of the analysis. Also shown in Fig. 4 is the anisotropy for the decreasing shear rate sweep for zero applied field. The differences in the anisotropy for the increasing and decreasing shear rate sweeps arise mostly due to preshearing of the dispersion along the z direction while loading into the cell. The differences may also be a consequence of the flow changing any flocculation in the dispersion.

At zero shear rate, application of a magnetic field causes a sharp increase in anisotropy, to 0.15 at $H=9$ mT and to 0.23 at $H=18$ mT. This increase suggests that the particles collectively undergo an orientational transition in which they tend to align in the magnetic field. When the dispersion is subjected to shear in a direction perpendicular to the magnetic field (i.e., along the x axis), the anisotropy decreases. The anisotropy decreases as the shear rate is increased from zero. However, at a particular shear rate, the anisotropy

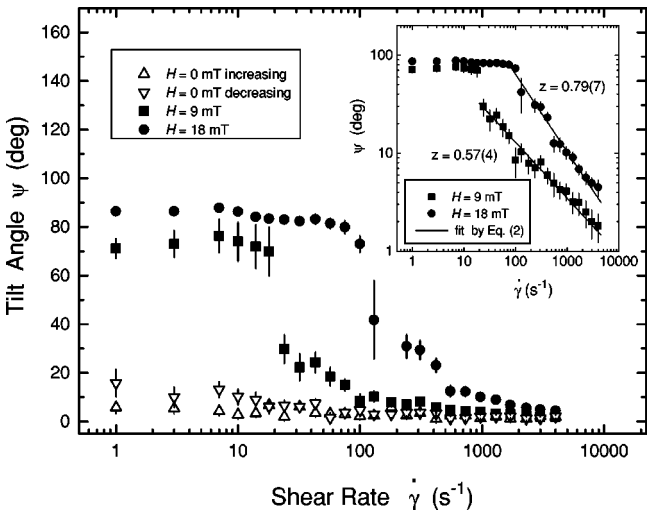

FIG. 5. The tilt angle ψ between the direction of shear flow and the direction of particle alignment as a function of shear rate in a 4.4 vol % magnetic dispersion for increasing shear rate sweep with no applied field, decreasing shear rate sweep with no applied field, applied field of 9 mT, and applied field of 18 mT. The inset shows the log-log plot of tilt angle vs the shear rate for measurements in applied field.

reaches a minimum and then increases with further increases in shear rate.

Figure 5 displays the tilt angle ψ as a function of shear rate for the four cases shown in Fig. 4. Note that at zero shear rate the anisotropy is effectively zero, so the tilt angle is indeterminate. Initiation of shear flow results in an increase in the anisotropy, and the tilt angle assumes values in the $0°-15°$ range. However, the tilt angle is remarkably independent of shear rate. At high shear rates the tilt angle obtained for the increasing and decreasing shear rate sweeps are equal within experimental error. At low shear rates, the difference becomes noticeable. As discussed above, this may be a consequence of long term relaxation or shear-induced changes in flocculation. However, the tilt angle becomes indeterminate in the limit of vanishing shear rate, because the anisotropy vanishes.

When a magnetic field is applied in the absence of shear flow, the tilt angle exhibits a sharp increase from its zero-field value to $87(1)°$ for $H=9$ mT, and to $91.1(12)°$ for $H=18$ mT. This suggests that the particles tend to be oriented in the direction of the field. In the presence of both shear flow and magnetic field transverse to the flow direction, the tilt angle remains at or near its zero-shear value until a characteristic shear rate is reached. Above this characteristic shear rate, which depends on the magnitude of the applied field ($18\ s^{-1}$ and $240\ s^{-1}$ in magnetic fields of 9 mT and 18 mT, respectively), the tilt angle decreases rapidly until it approaches the zero-field value. Comparison of Figs. 4 and 5 indicates that the anisotropy B/A reaches its minimum at the shear rate where the inflection point occurs in the plot of ψ as a function of $\dot{\gamma}$.

IV. DISCUSSION

The sharp rise of anisotropy and the tilt angle with the application of magnetic field suggests that a fraction of particles collectively undergo an orientational phase transition in which the particles become aligned along the magnetic field. Figure 5 demonstrates that an applied field of 18 mT is sufficient to align a significant fraction of particles along the field direction. Figures 4 and 5 demonstrate that, in the absence of magnetic field but under a shear flow, the particles tend to align in the flow direction. The alignment is very small at low shear rates and becomes substantial at higher shear rates.

When the magnetic dispersion is subjected to both shear flow and magnetic field, with the shear in a direction that is perpendicular to the magnetic field, the magnetic-field-induced anisotropy in orientation initially decreases with increasing shear rate. As the shear rate is increased, the anisotropy reaches a minimum and then starts to rise again. The small value of the anisotropy at the minimum indicates that the dispersion is in a nearly disordered state at this combination of shear and magnetic field. However, the tilt angle ψ remains nearly constant below a characteristic shear rate $\dot{\gamma}_c$. Above $\dot{\gamma}_c$, the tilt angle decreases with increasing shear rate. The observed shear rate dependence of anisotropy and tilt angle demonstrates an orientational transition from a field aligned state to a shear aligned state.

The inset to Fig. 5 indicates that the tilt angle as a function of shear rate above the characteristic shear rate follows a power law of the form

$$\psi = C\dot{\gamma}^{-z}, \tag{2}$$

where C is a proportionality constant and z is the dynamic exponent. The best fits, displayed by the solid lines over the data in the inset, yielded $C=178(26)$, $z=0.57(4)$ for $H=9$ mT and $C=2426(780)$, $z=0.79(7)$ for $H=18$ mT. These results show that the dynamic exponent depends on the strength of the magnetic field. The ratio of the exponents $z(H=18\ \text{mT})/z(H=9\ \text{mT})=1.4(2)$ compares quite well with the ratio 1.53 of B/A values at zero shear rate for the respective field values, suggesting that the dynamic exponent z depends on the degree of order in the dispersion obtained in the field at zero shear rate. Below the characteristic shear rate, the tilt angle does not depend on the shear rate.

A mean-field theory describes the orientational order in terms of an order parameter for this type of dispersion [14]. This theory uses an orientational distribution function $f(\mathbf{u},t)$, defined such that $f(\mathbf{u},t)d\mathbf{u}$ is the probability that a particle is within the solid angle $d\mathbf{u}$ of orientation $\mathbf{u}$ at time t. The model is based on a single-particle mean-field approach and treats the particles as rigid dumbbells dispersed in a solvent. It incorporates the effects of Brownian motion, anisotropic hydrodynamic drag, a steric (Maier-Saupe) potential, any external magnetic field, and a mean field for interparticle magnetic interactions. The model yields a diffusion equation that describes the time evolution of the orientation distribution function. To solve this equation, the distribution function is expanded in a series of spherical harmonics [21–23] and a set of evolution equations for the coefficients in the expansion is obtained. The coefficients are then found from the evolution equations and, finally, the distribution function. An orientational order tensor is defined as

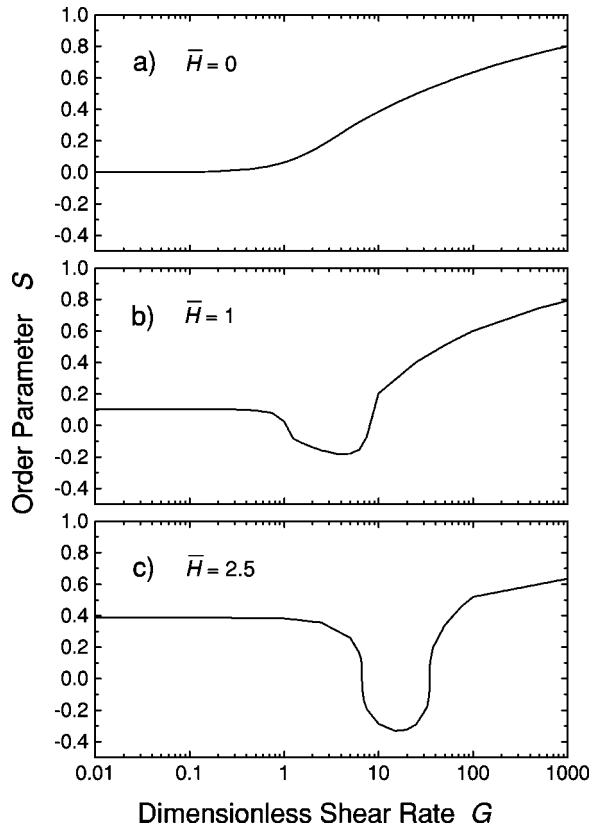

FIG. 6. Model predictions of the order parameter S as a function of dimensionless shear rate at various values of dimensionless applied field.

$$\mathbf{S} \equiv \int \left(\mathbf{uu} - \frac{1}{3}\delta \right) f(\mathbf{u}) d\mathbf{u}, \tag{3}$$

where δ is the second-order unit tensor. The scalar invariant

$$S = \left[\frac{9}{2} \mathrm{tr}(\mathbf{S} \cdot \mathbf{S} \cdot \mathbf{S}) \right]^{1/3} \tag{4}$$

gives a measure of the orientational order. A state of random order corresponds to $S=0$, and perfect alignment along a preferred direction corresponds to $S=1$. Negative S values denote oblate ordering (i.e., the states where the particles tend to align perpendicular to a preferred direction but are otherwise randomly oriented) and positive S values denote prolate ordering. For prolate ordering, we expect S to correlate with the anisotropy B/A.

In Fig. 6 we present the predictions of the model for S as a function of dimensionless shear rate ($G=6\lambda\dot{\gamma}/\sigma$) for several values of transverse magnetic field ($\bar{H}=\mu\mu_0 H/kT$). Note that $\bar{H}=1$ corresponds to $H\approx 1$ mT. In these expressions, σ is a positive constant describing the degree of anisotropy in the hydrodynamic force acting on a particle, μ is the magnetic moment of the particle, $\lambda=\zeta L^2/12kT$ is the time constant, L is the length of a rod, ζ is the scalar hydrodynamic drag coefficient for the particle, μ_0 is the permeability of free space, and kT is Boltzmann's constant times the temperature. The predictions in Fig. 6 for the order parameter and the results for the anisotropy in Fig. 4 are quite similar. At zero applied field, the model correctly predicts the general increase in order with increasing shear rate. In the presence of applied transverse magnetic field, the model predicts order at low shear rates, a decrease in order with increasing shear rate, and the reattainment of order at higher shear rates. However, the model predicts a more abrupt increase in order as the shear rate is increased through the less ordered state. These are most likely a consequence of the model not incorporating particle flocculation or a distribution of particle lengths.

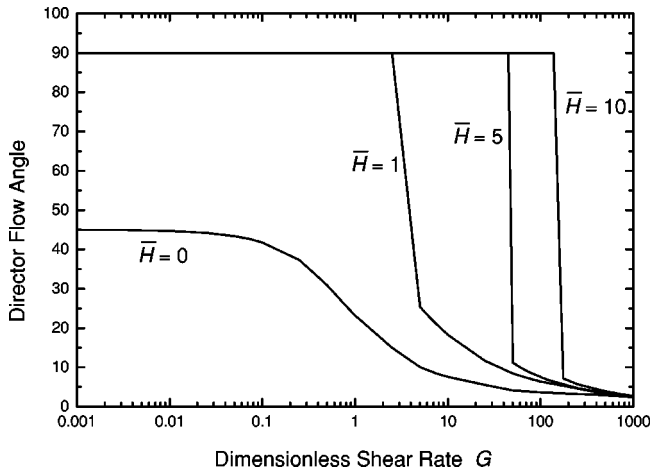

FIG. 7. Model predictions of the angle between the director and applied field as a function of dimensionless shear rate at various values of dimensionless applied field.

The model also gives predictions of the direction of average particle orientation through the principal eigenvector of **S**, the eigenvector that corresponds to the largest positive eigenvalue. In Fig. 7 we show predictions of the angle between the principal eigenvector (the director) and the flow direction as a function of shear rate for several values of a transverse magnetic field. The shear rate dependence of this angle qualitatively reproduces the features of the experimental ψ vs shear rate $\dot{\gamma}$ curves shown in Fig. 5. However, there is a notable difference between the experiment and the theory. The SANS experiments show that ψ varies smoothly with $\dot{\gamma}$, whereas this transition is predicted by the model to occur much more abruptly. We attribute this discrepancy mainly to the assumption in the model that all the particles are of the same size. If particles of different lengths undergo the transition at different shear rates, the transition would appear more smooth for a polydisperse system. The discrepancy is not entirely unexpected. Although we consider μ in the definition of $\bar{H}$ as being the moment of an individual particle, it is more likely that it is the moment of a primary aggregate such as a cluster of particles.

V. SUMMARY

Shear- and magnetic-field-induced orientational order in dispersions of acicular ferromagnetic nanoparticles has been

detected by small-angle neutron scattering. In the absence of flow, the magnetic field orients the particles in the field direction. In the absence of field, the flow orients the particles in the flow direction. When both flow and field are applied, the particle orientation depends on the relative magnitudes of the field and shear rate. Below a field-dependent characteristic shear rate, the field orientation dominates, and above this shear rate, flow orientation dominates. The competing effects of flow and magnetic field on particle alignment suggest that they can be used in combination to achieve desired states of nanoscale order in the dispersions. Model predictions agree qualitatively with the measured particle orientational behavior, with differences due to the model not including the effects of flocculation and/or nonuniform particle size.

ACKNOWLEDGMENTS

This project was supported by the National Science Foundation Materials Research Science and Engineering Center program through Grant Nos. DMR-9809423 and DMR-0213985, and the U.S. Department of Energy through Grant No. DE-FG02-02ER45966. This work is also based in part on activities supported by the National Science Foundation under Grant No. DMR-9986442. The authors would like to thank B. Greenwald and Y. Hernandez for their help during the SANS experiment.

[1] R.E. Rosenweig, *Ferrohydrodynamics* (Cambridge University Press, Cambridge, 1985).
[2] E. Blums, A. Cebers, and M.N. Maiorov, *Magnetic Fluids* (de Gruyters, New York, 1997).
[3] G.N. Coverdale, R.W. Chantrell, A. Satoh, and R. Vietch, J. Appl. Phys. **81**, 3818 (1997).
[4] S. Odenbach, T. Rylewicz, and M. Heyen, J. Magn. Magn. Mater. **201**, 155 (1999).
[5] *Magnetic Fluids and Applications Handbook*, edited by B.M. Berkovsky (Begell House, New York, 1996).
[6] K. O'Grady, R.G. Wilson, and P.C. Hobby, J. Magn. Magn. Mater. **95**, 341 (1991).
[7] C.D. Mee and E.D. Danial, *Magnetic Recording Technology*, 2nd ed. (McGraw-Hill, New York, 1996).
[8] M.-Carmen Miguel and R. Pastor-Satorras, Phys. Rev. E **59**, 826 (1999).
[9] H.W. Müller, Phys. Rev. Lett. **82**, 3907 (1999).
[10] W. Luo, T. Du, and J. Huang, Phys. Rev. Lett. **82**, 4134 (1999).
[11] D. Lacoste and T.C. Lubensky, Phys. Rev. E **64**, 041506 (2001).
[12] P.B. Visscher and Y. Günal, J. Appl. Phys. **81**, 3827 (1997).
[13] A. Satoh, J. Colloid Interface Sci. **234**, 425 (2001).
[14] A.S. Bhandar and J.M. Wiest, J. Colloid Interface Sci. **257**, 371 (2003).
[15] The identification of any commercial product or trade name does not imply endorsement or recommendation by the National Institute of Standards and Technology.
[16] C.D. Muzny, G.C. Straty, and H.J.M. Hanley, Phys. Rev. E **50**, R675 (1994).
[17] G.C. Straty, C.D. Muzny, B.D. Butler, M.Y. Lin, T.M. Slawecki, C.J. Glinka, and H.J.M. Hanley, Nucl. Instrum. Methods Phys. Res. A **408**, 511 (1998).
[18] See S. Kline, http://www.ncnr.nist.gov/programs/sans/manuals/data_red.html
[19] W. Wagner, A. Wiedenmann, W. Petry, A. Geibel, and H. Gleiter, J. Mater. Res. **6**, 2305 (1991).
[20] F. Gazeau, E. Dubois, J.-C. Bacri, F. Boue, A. Cebers, and R. Perzynski, Phys. Rev. E **65**, 031403 (2002).
[21] R.G. Larson, Macromolecules **23**, 3983 (1990).
[22] R.G. Larson and H.C. Öttinger, Macromolecules **24**, 6270 (1991).
[23] G. Marrucci and P.L. Maffettone, Macromolecules **22**, 4076 (1989).